

**Hugoniot equation-of-state and structure of laser-shocked polyimide C<sub>22</sub>H<sub>10</sub>N<sub>2</sub>O<sub>5</sub>**

K. Katagiri <sup>1,\*</sup> N. Ozaki <sup>1,2</sup> D. Murayama,<sup>1</sup> K. Nonaka,<sup>1</sup> Y. Hironaka,<sup>2,3</sup> Y. Inubushi,<sup>4,5</sup> K. Miyanishi <sup>5</sup>,  
H. Nakamura,<sup>1</sup> T. Okuchi <sup>6</sup> T. Sano <sup>2</sup> Y. Seto,<sup>7</sup> K. Shigemori <sup>2</sup> K. Sueda,<sup>5</sup> T. Togashi,<sup>4,5</sup>  
Y. Umeda <sup>6</sup> M. Yabashi <sup>4,5</sup> T. Yabuuchi,<sup>4,5</sup> and R. Kodama<sup>1,2</sup>

<sup>1</sup>Graduate School of Engineering, Osaka University, Osaka 565-0871, Japan

<sup>2</sup>Institute of Laser Engineering, Osaka University, Osaka 565-0871, Japan

<sup>3</sup>Open and Transdisciplinary Research Initiative, OTRI, Osaka University, Osaka 565-0871, Japan

<sup>4</sup>Japan Synchrotron Radiation Research Institute, Hyogo 679-5198, Japan

<sup>5</sup>RIKEN SPring-8 Center, Hyogo 679-5148, Japan

<sup>6</sup>Institute for Integrated Radiation and Nuclear Science, Kyoto University, Osaka 590-0494, Japan

<sup>7</sup>Graduate School of Science, Kobe University, Hyogo 657-0013, Japan



(Received 26 October 2021; revised 17 January 2022; accepted 27 January 2022; published 10 February 2022)

The Hugoniot equation-of-state, Grüneisen parameter, and structure of laser-shocked polyimide were measured. The polyimide Hugoniots were measured in the pressure range 80–600 GPa and found to be consistent with the extrapolation of previously reported data below 60 GPa. The structural measurements of polyimide shock compressed to pressures of 28–163 GPa were performed using the *in situ* x-ray diffraction technique, and the results show that the melting pressure of polyimide along its Hugoniot is below 32(±3) GPa, indicating that the discontinuous volume change of the polyimide Hugoniot at ~26 GPa observed in previous gas-gun experiments denotes the onset of melting. The consistency of the melting pressure between the previous gas-gun results and the present laser experiments suggests that the shock-melting process of polyimide is independent of the duration of the compression, revealing its rapid melting kinetics.

DOI: [10.1103/PhysRevB.105.054103](https://doi.org/10.1103/PhysRevB.105.054103)

**I. INTRODUCTION**

Among the numerous polymers found to date, polyimide (C<sub>22</sub>H<sub>10</sub>N<sub>2</sub>O<sub>5</sub>) has superior thermal, mechanical, and chemical properties due to the strong intermolecular forces of the *imide* bonds [1,2]. Understanding the shock responses of polyimide over a wide pressure range is important for the field of high-energy-density science, as polyimide is widely accepted as an ablator material in laser-shock experiments [3] and is also a candidate for the ablator material of the fuel capsule targets used in inertial confinement fusion research [4,5].

First Hugoniot (i.e., the locus of final shock states) measurements of polyimide were reported by Carter and Marsh in 1977 [6,7]. They shock-compressed polyimide with an initial density of 1.414 g/cm<sup>3</sup> to pressures up to 56 GPa using flyer plates driven by chemical explosives. Later, Ozaki *et al.* used shock waves induced by explosives or lasers to measure polyimide Hugoniot up to 65 GPa [8]. Although some nitrogen atoms in their polyimide were replaced by fluorine resulting in having a slightly higher initial density of 1.50 g/cm<sup>3</sup>, the reported Hugoniot is mostly consistent with the data of Carter and Marsh. They concluded that polyimide Hugoniot has a discontinuous density change at around 26 GPa, as also seen in the Hugoniot of Carter and Marsh. At the same time, the

same group reported results of polyimide Hugoniot measurements in a much higher and wider pressure range from 0.4 to 5.8 TPa [9], but the accuracy is not high, and the number of data is limited. More recently, Chen *et al.* reported Hugoniot of polyimide with an initial density of 1.35 g/cm<sup>3</sup> measured using a two-stage gas gun [10]. The measured pressure range was 9–43 GPa, and the results agree well with the data of Carter and Marsh. To summarize the previous data, although the Hugoniot of polyimide has been measured with high accuracy up to 60 GPa, there is a lack of data in the higher-pressure region.

Experimental determination of the structures of materials under shock is also important to understand their shock responses as such information gives direct evidence of structural transformations including melting. The existing polyimide Hugoniot has a discontinuous density change at a pressure of around 26 GPa, and this change might indicate the onset of melting of polyimide under shock. However, direct structural measurements using the *in situ* x-ray diffraction (XRD) technique are needed to unambiguously determine that this density jump is due to the melting. Such structural data of the ablator materials under shock is also necessary for the *in situ* x-ray diffraction experiments of the laser-shocked materials [11–13] to distinguish between the diffraction peaks from the sample of interest and those from the ablator material attached to the sample.

In this paper, we report the results of two independent laser-shock experiments on polyimide. One is the measurements of Hugoniot and Grüneisen parameters of polyimide

\*Corresponding author: [kkatagiri@ef.eie.eng.osaka-u.ac.jp](mailto:kkatagiri@ef.eie.eng.osaka-u.ac.jp)

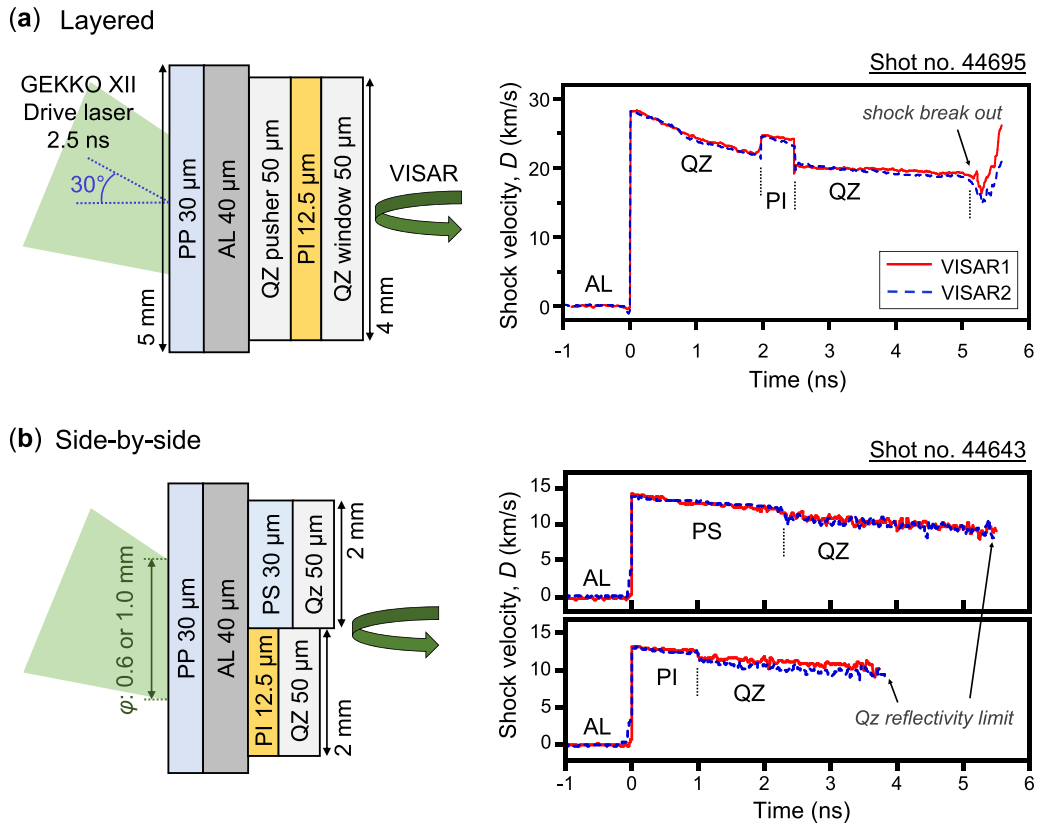


FIG. 1. Target configurations and typical velocity profiles of the GEKKO Hugoniot measurements. Two different target configurations, (a) *layered* and (b) *side-by-side*, were used for the Hugoniot measurements. The targets were consisted of polypropylene (PP), aluminum (AL), z-cut  $\alpha$  quartz (QZ), polystyrene (PS), and polyimide (PI).

using high-energy drive laser beams of GEKKO XII at the Institute of Laser Engineering, Osaka University. Another is *in situ* XRD measurements using the X-ray Free Electron Laser (XFEL) at SPring-8 Angstrom Compact Free Electron Laser (SACLA), observing the structure of the shock-compressed polyimide in the pressure range in and above the melting region.

## II. EXPERIMENT

### A. Hugoniot and reshock measurements

A polyimide film with a thickness of  $12.5 (\pm 0.1) \mu\text{m}$  (commercially available as Kapton® by Nilaco, product number 963181) was used, and its measured initial density was  $1.415 \text{ g/cm}^3$ . The experiments were performed using two types of shock targets as shown in Fig. 1. The target structures shown in Figs. 1(a) and 1(b) are hereafter referred to as the “layered” target and the “side-by-side” target, respectively. The shock velocities of polyimide, z-cut  $\alpha$  quartz, and polystyrene were time-resolved using a line-imaging velocity interferometer system for any reflector (VISAR) [14] operated with 532 nm probe light. The sensitivities of the two VISARs were 9.024 and 5.554 km/s/fringe in a vacuum, respectively. The field of view of the VISAR is  $\sim 600 \mu\text{m}$ . Both surfaces of the aluminum and quartz were polished. An antireflective coating for 532 nm wavelength was on the rear surface of the quartz to avoid the reflection of the probe light. The polyimide sample was dark yellow but the transmittance to the probe

light was high enough to perform the velocity measurements. For the refractive index  $n$  of polyimide at ambient conditions,  $n = 1.70$  is used [15].

Twelve high-energy laser beams of GEKKO XII [16] were used to drive a strong shock wave that compresses the shock targets. Three of the twelve beams had a spot size of  $1000 \mu\text{m}$  and a wavelength of 527 nm, and the other nine beams had a spot size of  $600 \mu\text{m}$  and a wavelength of 351 nm. The polyimide sample was shock compressed to different pressures from 80 to 600 GPa, by varying the number and energy of these laser beams. The drive laser pulse was a square in time with a full width at half maximum (FWHM) of 2.5 ns, and the rise and fall times were  $\sim 0.1$  ns each.

### B. X-ray diffraction measurements

The polyimide sample used in the XRD measurements was also from Nilaco (product number 963261) and its thickness was  $50.7 (\pm 0.3) \mu\text{m}$ . The drive laser with a wavelength of 532 nm installed at the Experimental Hatch 5 (EH5) of SACLA [17–19] was focused to the spot of  $\sim 170 \mu\text{m}$  diameter on the target to drive a single shock wave. The spot intensity pattern was smoothed by using a phase plate. The drive laser pulse was a square in time with a FWHM of 5 ns, and the rise and fall times were less than  $\sim 1$  ns each. The XFEL was irradiated 3.0 ns after the drive laser irradiation to collect the XRD pattern of the shocked polyimide. At the time of the x-ray probe,  $\sim 82\%$  and  $\sim 37\%$  of the sample depth

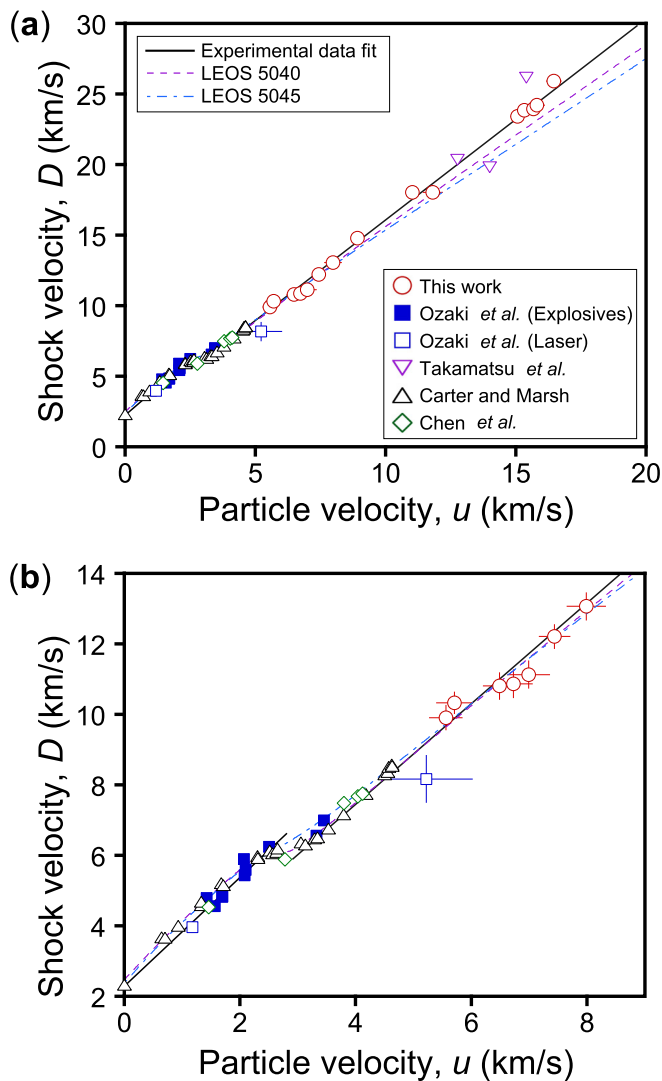


FIG. 2. (a) Particle velocity versus shock velocity of polyimide Hugoniot. Red open circles are the data obtained in this work. Other symbols are the data from previous reports [6–10]. The solid black lines are the fit of the data represented by Eqs. (3) and (4). The purple dashed line and light blue dot-dashed line are the LEOS 5040 and LEOS 5045 [27], respectively. (b) Detail of (a) in and above the melting point.

were compressed for the highest and the lowest pressure shots, respectively. The XFEL beam was focused to  $30 \times 10$  ( $W \times H$ )  $\mu\text{m}$  and was incident on the target at an angle of  $\chi = 108^\circ$ . The photon energy was 11.0 keV and the number of photons was  $\sim 10^{11}$  photons/pulse. The diffracted x rays were collected on a two-dimensional x-ray detector in reflection geometry. The recorded XRD images were analyzed by using IPAnalyzer and PDIndexer [20,21]. The diffracted x rays recorded at azimuthal angles ( $\varphi$ ) of  $-5 \leq \varphi \leq 5$  degrees were integrated to analyze the structures of shocked polyimide. Here, the shock wave propagation direction is assumed to be along  $\varphi = 0^\circ$ .

VISAR measurements using a probe light with 515 nm wavelength were also performed simultaneously to measure the timing of the shock wave breaking out from the rear surface of the polyimide to the vacuum. The transit time of

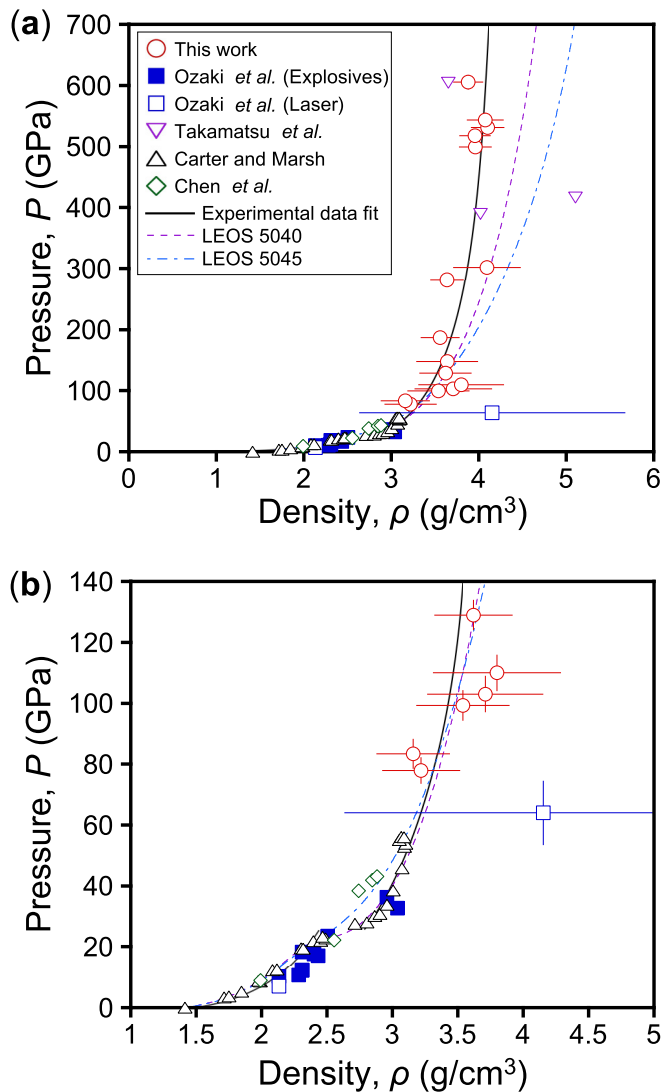


FIG. 3. (a) Density versus pressure of polyimide Hugoniot. The symbols and coloration are the same as in Fig. 2. The solid black curves are the experimental data fit obtained from Eqs. (3) and (4) using  $\rho_0 = 1.415$  as the initial density. (b) Detail of (a) in and above the melting point.

the shock wave propagating in the polyimide is determined by the recorded break-out timing and the drive laser irradiation timing which is estimated from the calibration shots [22]. Then the average shock velocity is obtained by dividing the initial sample thickness by the estimated transit time. The pressure in polyimide is estimated from the obtained average shock velocity through the polyimide Hugoniot which is also reported in this work. From the VISAR measurements, the pressures achieved in the XRD experiments were estimated to range from  $28(\pm 4)$  to  $163(\pm 16)$  GPa.

### III. RESULTS AND DISCUSSION

#### A. Hugoniot

The compression states of polyimide were determined from the obtained shock velocities by using the impedance mismatching method [23]. The quartz [24], polystyrene [25],

TABLE I. Summary of the shock data obtained in the polyimide Hugoniot measurements. The  $D$ ,  $u$ ,  $P$ , and  $\rho$  are the shock velocity, particle velocity, pressure, and density, respectively. The subscripts  $PI$ ,  $QZ$ , and  $PS$  denote the polyimide, quartz, and polystyrene, respectively.

Shot no.	Target Configuration	$D_{PI}$ (km/s)	$D_{QZ}^a$ (km/s)	$D_{PS}$ (km/s)	$u_{PI}$ (km/s)	$P_{PI}$ (GPa)	$\rho_{PI}$ (g/cm <sup>3</sup> )
44725	side-by-side	9.91 ± 0.36		10.45 ± 0.30	5.56 ± 0.29	77.9 ± 4.4	3.22 ± 0.30
44723	side-by-side	10.3 ± 0.3		10.70 ± 0.35	5.71 ± 0.32	83.4 ± 4.9	3.16 ± 0.28
44660	side-by-side	10.8 ± 0.4		11.69 ± 0.30	6.49 ± 0.29	99.3 ± 5.0	3.54 ± 0.36
44641	side-by-side	10.9 ± 0.4		11.97 ± 0.34	6.73 ± 0.33	103 ± 6	3.71 ± 0.44
44665	side-by-side	11.1 ± 0.4		12.32 ± 0.40	6.99 ± 0.37	110 ± 6	3.80 ± 0.49
44643	side-by-side	13.1 ± 0.4		13.84 ± 0.37	7.99 ± 0.34	148 ± 7	3.64 ± 0.35
44628	layered	12.2 ± 0.4	12.18 ± 0.28		7.44 ± 0.27	129 ± 5	3.62 ± 0.30
44666	layered	14.8 ± 0.4	14.13 ± 0.22		8.92 ± 0.23	187 ± 6	3.56 ± 0.22
44706	layered	18.1 ± 0.3	16.71 ± 0.24		11.0 ± 0.3	282 ± 8	3.64 ± 0.19
44629	layered	18.1 ± 0.5	17.45 ± 0.35		11.8 ± 0.4	302 ± 11	4.10 ± 0.39
44726	layered	23.4 ± 0.4	21.29 ± 0.24		15.1 ± 0.3	499 ± 10	3.96 ± 0.19
44709	layered	23.9 ± 0.3	21.60 ± 0.26		15.3 ± 0.3	518 ± 11	3.96 ± 0.18
44698	layered	23.9 ± 0.3	21.93 ± 0.25		15.7 ± 0.3	531 ± 11	4.10 ± 0.19
44695	layered	24.2 ± 0.4	22.09 ± 0.27		15.8 ± 0.3	542 ± 12	4.07 ± 0.21
44626	layered	25.9 ± 0.4	22.95 ± 0.26		16.5 ± 0.3	604 ± 12	3.88 ± 0.17

<sup>a</sup> $D_{QZ}$  is the shock velocity in the first quartz obtained at the interface between the first quartz and polyimide.

and aluminum [26] were used as the pressure standard materials for the impedance mismatching analysis. The pressure  $P$  and density  $\rho$  at its shocked (Hugoniot) state are related with the shock velocity  $D$  and particle velocity  $u$ , through the Rankine-Hugoniot equations:

$$P - P_0 = \rho_0 D u, \quad (1)$$

$$\rho = \rho_0 \frac{D}{D - u}, \quad (2)$$

where  $P_0$  and  $\rho_0$  are the pressure and density before the shock compression.

The measured  $D$ - $u$  and  $P$ - $\rho$  relationships of shocked polyimide are shown in Figs. 2 and 3, respectively. See Table I also for the summarized shock data collected for the Hugoniot measurements. The errors on  $D$  include the 5% of the velocity sensitivities and the standard deviation of the velocities read from several different fringes. The errors on  $u$ ,  $P$ , and  $\rho$  are the estimation of the 1-sigma uncertainties propagated from the uncertainties on shock velocities of polyimide and standard materials by performing a Monte Carlo calculation with 10 000 runs for each data point.

Our polyimide Hugoniots agree with the extrapolation of the previously reported data of Carter and Marsh, Chen *et al.*, and Ozaki *et al.*, except one outlier at  $u \sim 5$  km/s from Ozaki *et al.* Ozaki *et al.* used two different types of drivers and most of the data were taken by using explosives which was a conventional and reliable method to measure Hugoniot. The outlier was, however, collected by using optical lasers as the driver and this resulted in less accuracy as the large error bars on the plot shows. Therefore, the difference between the present Hugoniot data and the outlier of Ozaki *et al.* should be due to the large uncertainties in their measurements. Indeed, the deviation of their outlier point from our data is within the error bars. The Hugoniot points from Takamatsu *et al.* are also shown in Figs. 2 and 3. Their data are in rough agreement

with ours, but we do not discuss it further as the accuracy of their data is not high, and they do not report the experimental uncertainties on their data. Note that the driver used in our experiments is also optical lasers, but the use of the VISAR systems allows us to perform velocity measurements with much higher accuracy than in the previous studies.

Together with the data reported in previous works of Carter and Marsh [6,7], Chen *et al.* [10], and Ozaki *et al.* (excluding their laser-shock data) [8], the measured polyimide Hugoniot is characterized by  $D - u$  relationships by the general form of  $D = C_0 + S u$  as

$$D = 2.327 + 1.55(\pm 0.06) \times u, \text{ for } u < 2.78 \text{ km/s}, \quad (3)$$

$$D = 1.79(\pm 0.11) + 1.43(\pm 0.02) \times u, \text{ for } u \geq 2.78 \text{ km/s}. \quad (4)$$

Here, the bulk sound speed of polyimide at ambient conditions  $V_\phi = 2.327$  km/s from Ref. [7] is used for the  $C_0$  of Eq. (3). The discontinuous density change observed at  $u \sim 2.78$  km/s ( $P \sim 26$  GPa) in previous studies [6–8,10] denotes the melt onset, as the XRD results described in Sec. III C demonstrate.

## B. Reshock

When the shock wave propagating in the polyimide enters the quartz window, the polyimide is reshocked by the reflected wave propagating backward, since the shock impedance of quartz is higher than that of polyimide. The reshock path of a material is often approximated by the reflection of its principal Hugoniot in the  $P$ - $u$  plane. The actual reshock path is, however, slightly different from the reflected Hugoniot and this small deviation can be estimated by the Grüneisen parameter. Since the Hugoniot of quartz is already known accurately [24], the Grüneisen parameter of shocked polyimide can be determined by measuring the shock velocities of polyimide and quartz at their interface.

TABLE II. Summary of the reshock data of polyimide. The  $D_{PI,2}$  is the shock velocity of polyimide immediately before the shock enters the quartz window. The  $D_{QZ,2}$  is the shock velocity of quartz window immediately after the shock enters from the polyimide. The  $V$  is the volume of polyimide at the reshock state. The  $\gamma$  is the determined Grüneisen parameter of polyimide at  $V$ . The quartz window did not show sufficient reflectivity in the shots not listed here but listed in Table I.

Shot no.	Target Configuration	$D_{PI,2}$ (km/s)	$D_{QZ,2}$ (km/s)	$V$ (cm <sup>3</sup> /g)	$\gamma$
44643	side-by-side	12.6 ± 0.5	11.40 ± 0.73	0.18 ± 0.08	0.67 ± 0.36
44666	layered	14.3 ± 0.5	12.88 ± 0.80	0.19 ± 0.06	0.72 ± 0.28
44706	layered	17.9 ± 0.8	15.44 ± 0.93	0.14 ± 0.10	0.45 ± 0.35
44629	layered	17.9 ± 0.5	15.79 ± 0.45	0.18 ± 0.04	0.66 ± 0.17
44726	layered	22.9 ± 0.6	<sup>a</sup>		
44709	layered	23.3 ± 0.6	20.38 ± 0.84	0.20 ± 0.03	0.75 ± 0.15
44698	layered	23.4 ± 0.5	20.05 ± 0.59	0.17 ± 0.03	0.85 ± 0.35
44695	layered	23.6 ± 0.5	20.40 ± 0.47	0.18 ± 0.03	0.61 ± 0.13
44626	layered	25.1 ± 0.6	21.78 ± 0.61	0.20 ± 0.03	0.72 ± 0.13

<sup>a</sup>Shock velocity not accurately measured. A strong reflection from the rear surface of the quartz window interfered with the measurement.

From the measured Hugoniot pressure of the quartz window  $P_{QZ}$  and the Hugoniot pressures of polyimide at a given volume  $P_{PI}$ , the Grüneisen parameter  $\gamma$  of polyimide can be determined by [28,29]

$$\gamma = \frac{2V[P_{PI}(V) - P_{QZ}]}{(V_0 - V)[P_{PI}(V) - P_{PI}(V_1)] - (V_1 - V)P_{QZ}}, \quad (5)$$

where  $V_0$ ,  $V_1$ , and  $V$  are the volumes of the polyimide before compression, at the first shock state, and at the reshock state, respectively. The  $V$  is given by

$$V = V_1 - \frac{[u_{PI}(V_1) - u_{QZ}]^2}{P_{QZ} - P_{PI}(V_1)}, \quad (6)$$

where  $u_{PI}(V_1)$  is the particle velocity of the polyimide at the first shock state and  $u_{QZ}$  is the particle velocity of the quartz window.

The determined Grüneisen parameter of polyimide are listed in Table II along with the measured shock velocities of polyimide and quartz window at their interface. As shown in Fig. 1, the shock is weakly decaying as it propagates in the polyimide, and thus the measured shock velocity of polyimide immediately before it enters the quartz window (i.e.,  $D_{PI,2}$  in Table II) is slower than that measured immediately after the shock enters polyimide from the pusher (i.e.,  $D_{PI}$  in Table I). Therefore, the  $P_{PI}(V_1)$  and  $u_{PI}(V_1)$  in Eqs. (5) and (6) are estimated from the measured  $D_{PI,2}$  using the polyimide Hugoniot measured in this work [i.e., Eq. (4)]. Figure 4 shows the volume dependence of the Grüneisen parameter. The relationship between the Grüneisen parameter and volume under shock is often approximated by  $\gamma(V) = \gamma_0(V/V_0)^q$ . After fitting our plots,  $q = 0.59(\pm 0.04)$  is obtained for the measured Grüneisen parameter of shocked polyimide, which is consistent with the previously reported gas-gun data at higher  $V/V_0$ .

### C. X-ray diffraction

Typical XRD images of shocked polyimide are shown in Fig. 5 along with an unshocked image and the experimental schematic. All the XRD profiles obtained in this work are summarized in Fig. 6(a) and the XRD profiles with the un-compressed fraction subtracted are shown in Fig. 6(b). The

compressed fraction of polyimide at the time of the XFEL probe (3 ns after the drive laser irradiation) is estimated from the initial sample thickness and shock transit time (see Table III). Here, the shock velocity is assumed to be steady in time as the decaying ratio is not observable in this scheme. In Fig. 6, the length of the scattering vector  $k = 4\pi \sin\theta/\lambda$  is calculated for the probe pulse wavelength  $\lambda = 1.127 \text{ \AA}$ .

Previous studies suggested the existence of a discontinuous change in density at  $\sim 26 \text{ GPa}$  on the polyimide Hugoniot [6–8,10] and our XRD results showing typical liquid features at pressures of 32 GPa or higher indicate that this density change is due to melting. As shown in Fig. 6(b), the structure of polyimide observed at 28 GPa is different from those observed at higher pressures as the first peak observed for the 28 GPa shot appears at lower  $k$  to be compared to the typical

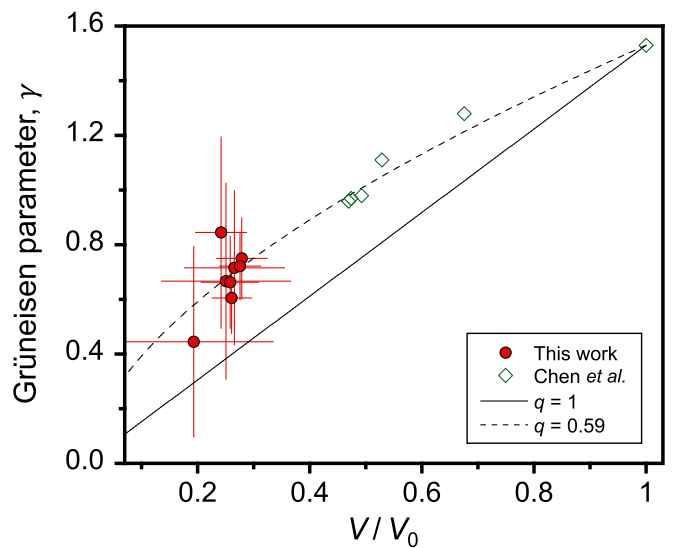


FIG. 4. Grüneisen parameter of polyimide. The green open diamonds are the previously reported gas-gun data [10]. The Grüneisen parameter at the initial state is  $\gamma_0 = 1.53$  [10]. The  $\gamma-V/V_0$  relationships expressed by  $\gamma(V) = \gamma_0(V/V_0)^q$  are also shown for  $q = 1$  (black solid line) and  $q = 0.59$  (black dashed curve).

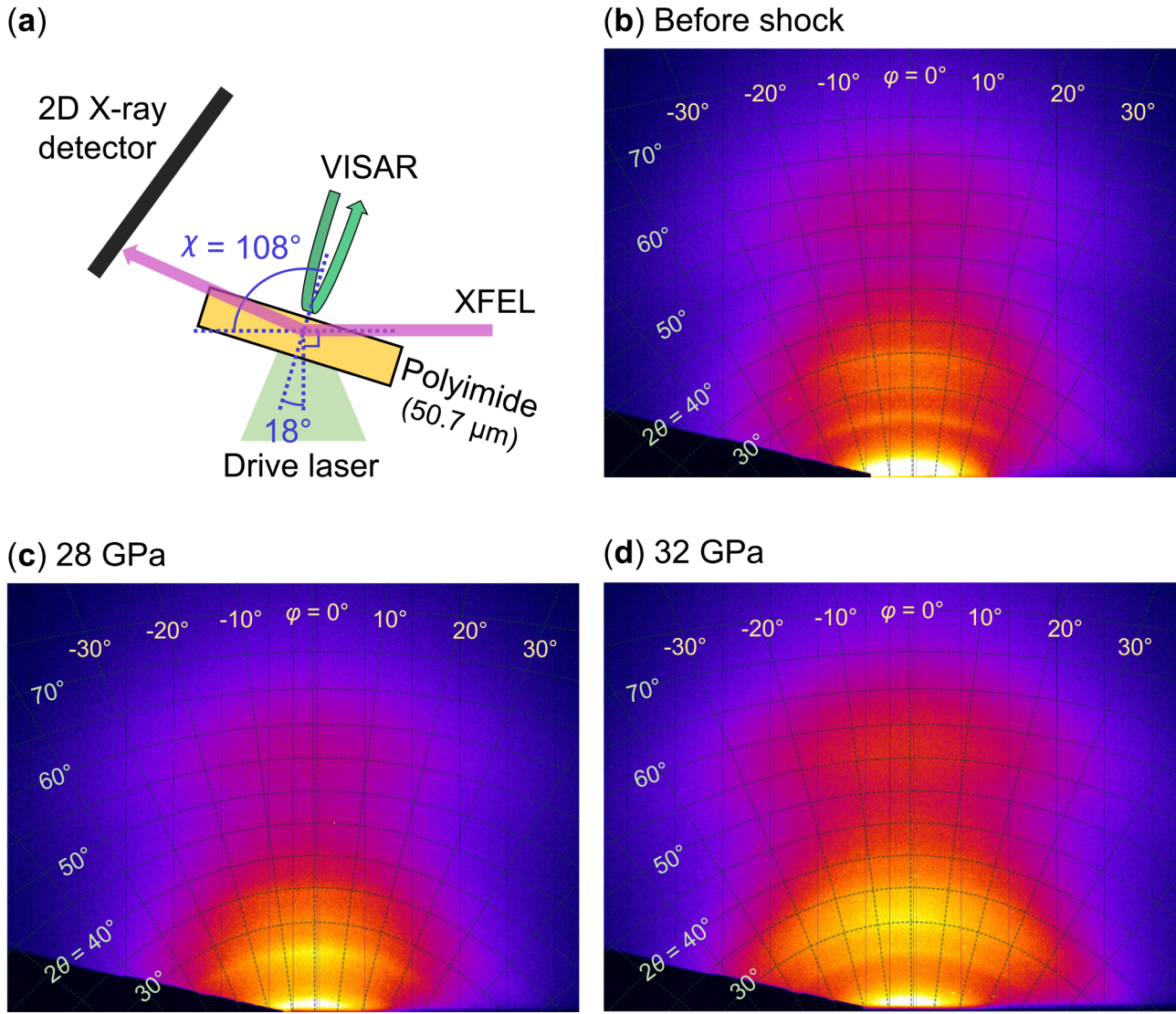


FIG. 5. (a) Experimental configuration of the SACLA XRD measurements. (b) XRD diffraction pattern from the polyimide sample before shock. (c), (d) The raw XRD images of shocked polyimide obtained at (c) 28 GPa and (d) 32 GPa. The dotted curves and lines in (b)–(d) show the constant scattering angle ( $2\theta$ ) and azimuthal angle ( $\varphi$ ), respectively.

liquid diffraction features observed at higher pressures. Also, the second broad peak ( $k \sim 5.5 \text{ \AA}^{-1}$ ) observed at 32 GPa or higher is absent for the 28 GPa profile. These differences suggest that polyimide is not completely melted at 28 GPa. The consistency between the gas-gun results and the laser experiments suggests that the melting of polyimide completes

quickly and does not depend much on the duration of the compression.

Since the shock velocity increases with increasing pressure and the x-ray probe timing was set to a constant value of 3.0 ns for all the shots taken, the fraction of the compressed volume probed by x rays increases as the pressure increases.

TABLE III. Summary of the shock data obtained in the XRD measurements. The  $D$  is the average shock velocity and  $P$  is the corresponding shock pressure of polyimide.

Shot no.	Shock Transit Time (ns)	$D$ (km/s)	$P$ (GPa)	Compressed Fraction at the Time of Probe (%)
956926	$8.01 \pm 0.61$	$6.33 \pm 0.49$	$28 \pm 4$	$37 \pm 3$
956932	$7.62 \pm 0.48$	$6.65 \pm 0.42$	$32 \pm 3$	$39 \pm 2$
956944	$7.34 \pm 0.38$	$6.91 \pm 0.36$	$35 \pm 3$	$41 \pm 2$
956946	$4.88 \pm 0.34$	$10.4 \pm 0.74$	$88 \pm 10$	$61 \pm 4$
956390	$3.68 \pm 0.24$	$13.8 \pm 0.89$	$163 \pm 16$	$82 \pm 5$

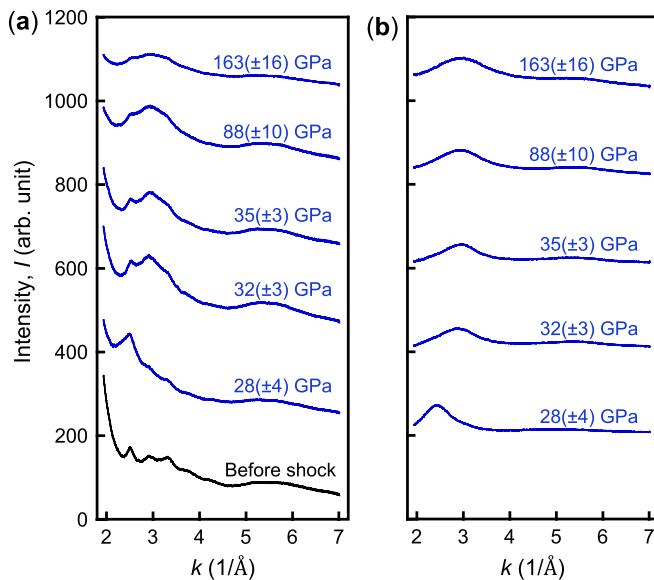


FIG. 6. (a) The raw XRD lineouts of shocked (blue) and unshocked (black) polyimide. Shown uncertainties of pressures are propagated from the estimated uncertainties on the average shock velocities. (b) The results with the uncompressed fraction of polyimide subtracted from the profiles shown in (a). The shot-by-shot fluctuation of the XFEL pulse energy is collected for (b) before subtracting the unshocked fraction.

This causes the liquid peaks to become more pronounced at higher pressures. The positions of the observed liquid peaks do not shift significantly by increasing the pressure from 32 to 163 GPa, suggesting that the density of the shock melted polyimide does not increase much with increasing pressure. This is consistent with the polyimide Hugoniot measured in the GEKKO experiments, which shows the compressibility does not increase much above the melting pressure.

#### IV. SUMMARY

Measurements of Hugoniot EOS, Grüneisen parameter, and structures of shock-compressed polyimide are reported.

The reported Hugoniot and Grüneisen parameter can be used for the prediction and experimental determination of the single- and double-shocked state of polyimide. The *in situ* XRD observations of shocked polyimide showed that the melting pressure of polyimide under shock is lower than  $32(\pm 3)$  GPa, indicating that the discontinuous density change on the polyimide Hugoniot at around 26 GPa denotes the onset of melting. Recent *in situ* XRD measurements on shocked polymers [30–34] revealed several interesting phenomena, such as the mixing and demixing of carbon and hydrogen atoms [30] and the formation of diamond in double shocked polystyrene [31–33]. Such changes in structures and physical properties of polymers under high pressure are important research topics to be further studied.

#### ACKNOWLEDGMENTS

We thank Dr. M. Millot for providing the LEOS data, Y. Muramatsu and M. Yamagishi for their assistance in target preparations, and the technical staff of GEKKO and SACLA for their support during the experiments. The Hugoniot measurements were conducted under the joint research of the Institute of Laser Engineering, Osaka University, Japan. The XRD experiments were performed at BL3 of SACLA with the approval of the Japan Synchrotron Radiation Research Institute (Proposals No. 2020A8033 and No. 2020A8048). These works were supported by grants from MEXT Quantum Leap Flagship Program (MEXT Q-LEAP), Grant No. JPMXS0118067246, Japan Society for the Promotion of Science (JSPS) KAKENHI (Grants No. 21J10604, No. 20H00139, and No. 19K21866), and Genesis Research Institute, Inc. (Konpon-ken, Toyota). The part of the results was obtained using a high-power nanosecond laser deployed at SACLA by Institute of Laser Engineering of Osaka University with the corporation of Hamamatsu Photonics. The installation of Diffractive Optical Elements (DOE) to improve the smoothness of the drive laser pattern was supported by the SACLA Basic Development Program.

- [1] M. K. Ghosh and K. L. Mittal, *Polyimide: Fundamentals and Applications* (Marcel Dekker, New York, 1996).
- [2] D. J. Liaw, K. L. Wang, Y. C. Huang, K. R. Lee, J. Y. Lai, and C. S. Ha, *Prog. Polym. Sci.* **37**, 907 (2012).
- [3] M. C. Akin, D. E. Fratanduono, and R. Chau, *J. Appl. Phys.* **119**, 045901 (2016).
- [4] T. R. Dittrich, S. W. Haan, M. M. Marinak, S. M. Pollaine, D. E. Hinkel, D. H. Munro, C. P. Verdon, G. L. Strobel, R. McEachern, R. C. Cook, C. C. Roberts, D. C. Wilson, P. A. Bradley, L. R. Foreman, and W. S. Varnum, *Phys. Plasmas* **6**, 2164 (1999).
- [5] D. Marsacq, B. Dufour, B. Blondel, Y. Lavergne, and G. Thevenot, *Polym. Int.* **49**, 1021 (2000).
- [6] W. J. Carter and S. P. Marsh, LANL, Technical Report No. LA-13006-MS, Los Alamos, 1977.
- [7] S. P. Marsh, *LASL Shock Hugoniot Data* (University of California Press, Berkeley, 1980).
- [8] N. Ozaki, K. A. Tanaka, Y. Sasatani, K. Fujita, K. Takamatsu, M. Nakano, M. Yoshida, K. Okada, E. Takahashi, Y. Owadano, H. Takenaka, and K. Kondo, *Phys. Plasmas* **10**, 2475 (2003).
- [9] K. Takamatsu, N. Ozaki, K. A. Tanaka, T. Ono, K. Nagai, M. Nakai, T. Watari, A. Sunahara, M. Nakano, T. Kataoka, H. Takenaka, M. Yoshida, K. Kondo, and T. Yamanaka, *Phys. Rev. E* **67**, 056406 (2003).
- [10] H. Chen, W. H. Tang, X. W. Ran, M. Zhang, and Z. Xu, *Chin. Sci. Bull.* **58**, 585 (2013).
- [11] M. O. Schoelmerich, T. Tschentscher, S. Bhat, C. A. Bolme, E. Cunningham, R. Farla, E. Galtier, A. E. Gleason, M. Harmand, Y. Inubushi, K. Katagiri, K. Miyanishi, B. Nagler, N. Ozaki, T. R. Preston, R. Redmer, R. F. Smith, T. Tobase, T. Togashi, S. J. Tracy *et al.*, *Sci. Rep.* **10**, 10197 (2020).
- [12] S. M. Sharma, S. J. Turneure, J. M. Winey, P. A. Rigg, N. Sinclair, X. Wang, Y. Toyoda, and Y. M. Gupta, *Phys. Rev. X* **10**, 011010 (2020).

- [13] S. J. Turneaure, S. M. Sharma, and Y. M. Gupta, *Phys. Rev. Lett.* **125**, 215702 (2020).
- [14] P. M. Celliers, D. K. Bradley, G. W. Collins, and D. G. Hicks, *Rev. Sci. Instrum.* **75**, 4916 (2004).
- [15] S. S. Hardaker, S. Moghazy, C. Y. Cha, and R. J. Samuels, *J. Polym. Sci. B: Polym. Phys.* **31**, 1951 (1993).
- [16] N. Ozaki, K. A. Tanaka, T. Ono, K. Shigemori, M. Nakai, H. Azechi, T. Yamanaka, K. Wakabayashi, M. Yoshida, H. Nagao, and K. Kondo, *Phys. Plasmas* **11**, 1600 (2004).
- [17] Y. Inubushi, T. Yabuuchi, T. Togashi, K. Sueda, K. Miyanishi, Y. Tange, N. Ozaki, T. Matsuoka, R. Kodama, T. Osaka, S. Matsuyama, K. Yamauchi, H. Yumoto, T. Koyama, H. Ohashi, K. Tono, and M. Yabashi, *Appl. Sci.* **10**, 2224 (2020).
- [18] Y. Inubushi, I. Inoue, J. Kim, A. Nishihara, S. Matsuyama, H. Yumoto, T. Koyama, K. Tono, H. Ohashi, K. Yamauchi, and M. Yabashi, *Appl. Sci.* **7**, 584 (2017).
- [19] T. Ishikawa *et al.*, *Nat. Photon.* **6**, 540 (2012).
- [20] Y. Seto, IPAnalyzer, <https://github.com/seto77/IPAnalyzer/>.
- [21] Y. Seto, PDIndexer, <https://github.com/seto77/PDIndexer/>.
- [22] K. Katagiri, N. Ozaki, S. Ohmura, B. Albertazzi, Y. Hironaka, Y. Inubushi, K. Ishida, M. Koenig, K. Miyanishi, H. Nakamura, M. Nishikino, T. Okuchi, T. Sato, Y. Seto, K. Shigemori, K. Sueda, Y. Tange, T. Togashi, Y. Umeda, M. Yabashi *et al.*, *Phys. Rev. Lett.* **126**, 175503 (2021).
- [23] Y. B. Zel'dovich and Y. P. Raizer, *Physics of Shock Waves and High-Temperature Hydrodynamic Phenomena* (Academic Press, New York, 1966).
- [24] M. P. Dejarlais and M. D. Knudson, *J. Appl. Phys.* **122**, 035903 (2017).
- [25] C. A. McCoy, S. X. Hu, M. C. Marshall, D. N. Polsin, D. E. Fratanduono, Y. H. Ding, P. M. Celliers, T. R. Boehly, and D. D. Meyerhofer, *Phys. Rev. B* **102**, 184102 (2020).
- [26] M. D. Knudson and M. P. Desjarlais, *Phys. Rev. B* **88**, 184107 (2013).
- [27] M. Millot (private communication).
- [28] D. G. Hicks, T. R. Boehly, P. M. Celliers, D. K. Bradley, J. H. Eggert, R. S. McWilliams, R. Jeanloz, and G. W. Collins, *Phys. Rev. B* **78**, 174102 (2008).
- [29] L. E. Crandall, J. R. Rygg, D. K. Spaulding, M. F. Huff, M. C. Marshall, D. N. Polsin, R. Jeanloz, T. R. Boehly, M. Zaghoo, B. J. Henderson, S. Brygoo, P. M. Celliers, J. H. Eggert, D. E. Fratanduono, A. Lazicki, M. Millot, and G. W. Collins, *Phys. Plasmas* **28**, 022708 (2021).
- [30] N. J. Hartley, J. Grenzer, L. Huang, Y. Inubushi, N. Kamimura, K. Katagiri, R. Kodama, A. Kon, W. Lu, M. Makita, T. Matsuoka, S. Nakajima, N. Ozaki, T. Pikuz, A. V. Rode, D. Sagae, A. K. Schuster, K. Tono, K. Voigt, J. Vorberger *et al.*, *Phys. Rev. Lett.* **121**, 245501 (2018).
- [31] D. Kraus, J. Vorberger, A. Pak, N. J. Hartley, L. B. Fletcher, S. Frydrych, E. Galtier, E. J. Gamboa, D. O. Gericke, S. H. Glenzer, E. Granados, M. J. MacDonald, A. J. MacKinnon, E. E. McBride, I. Nam, P. Neumayer, M. Roth, A. M. Saunders, A. K. Schuster, P. Sun *et al.*, *Nat. Astron.* **1**, 606 (2017).
- [32] D. Kraus, N. J. Hartley, S. Frydrych, A. K. Schuster, K. Rohatsch, M. Rödel, T. E. Cowan, S. Brown, E. Cunningham, T. van Driel, L. B. Fletcher, E. Galtier, E. J. Gamboa, A. Laso Garcia, D. O. Gericke, E. Granados, P. A. Heimann, H. J. Lee, M. J. MacDonald, A. J. MacKinnon *et al.*, *Phys. Plasmas* **25**, 056313 (2018).
- [33] A. K. Schuster, N. J. Hartley, J. Vorberger, T. Döppner, T. van Driel, R. W. Falcone, L. B. Fletcher, S. Frydrych, E. Galtier, E. J. Gamboa, D. O. Gericke, S. H. Glenzer, E. Granados, M. J. MacDonald, A. J. MacKinnon, E. E. McBride, I. Nam, P. Neumayer, A. Pak, I. Prencipe *et al.*, *Phys. Rev. B* **101**, 054301 (2020).
- [34] J. Lütgert, J. Vorberger, N. J. Hartley, K. Voigt, M. Rödel, A. K. Schuster, A. Benuzzi-Mounaix, S. Brown, T. E. Cowan, E. Cunningham, T. Döppner, R. W. Falcone, L. B. Fletcher, E. Galtier, S. H. Glenzer, A. Laso Garcia, D. O. Gericke, P. A. Heimann, H. J. Lee, E. E. McBride *et al.*, *Sci. Rep.* **11**, 12883 (2021).